Instruments and Methods

Using distributed temperature sensors to monitor an Antarctic ice shelf and sub-ice-shelf cavity

S.W. TYLER,[1] D.M. HOLLAND,[2] V. ZAGORODNOV,[3] A.A. STERN,[2] C. SLADEK,[1] S. KOBS,[1] S. WHITE,[4] F. SUÁREZ,[5] J. BRYENTON[6]

[1]Department of Geological Sciences and Engineering, University of Nevada, Reno, NV, USA
E-mail: styler@unr.edu
[2]Courant Institute of Mathematical Sciences, New York University, New York, NY, USA
[3]Byrd Polar Research Center, The Ohio State University, Columbus, OH, USA
[4]UNAVCO, Boulder, CO, USA
[5]Department of Hydraulic and Environmental Engineering, Pontificia Universidad Católica de Chile, Santiago, Chile
[6]Lockheed Martin Company, Centennial, CO, USA

ABSTRACT. Monitoring of ice-shelf and sub-ice-shelf ocean temperatures represents an important component in understanding ice-sheet stability. Continuous monitoring is challenging due to difficult surface access, difficulties in penetrating the ice shelf, and the need for long-term operation of non-recoverable sensors. We aim to develop rapid lightweight drilling and near-continuous fiber-optic temperature-monitoring methods to meet these challenges. During November 2011, two instrumented moorings were installed within and below the McMurdo Ice Shelf (a sub-region of the Ross Ice Shelf, Antarctica) at Windless Bight. We used a combination of ice coring for the upper portion of each shelf borehole and hot-point drilling for penetration into the ocean. The boreholes provided temporary access to the ice-shelf cavity, into which distributed temperature sensing (DTS) fiber-optic cables and conventional pressure/temperature transducers were installed. The DTS moorings provided near-continuous (in time and depth) observations of ice and ocean temperatures to a depth of almost 800 m beneath the ice-shelf surface. Data received document the presence of near-freezing water throughout the cavity from November through January, followed by an influx of warmer water reaching ∼150 m beneath the ice-shelf base during February and March. The observations demonstrate prospects for achieving much higher spatial sampling of temperature than more conventional oceanographic moorings.

INTRODUCTION

The interaction between the ocean and floating ice shelves is widely recognized as a critical process in the future of the contribution of the Antarctic and Greenland ice sheets to global sea level (e.g. Jacobs and others, 2011; Hattermann and others, 2012; Hellmer and others, 2012). Yet much of this interaction occurs beneath the ice shelves where measurement of both glacial and ocean processes is most challenging and least probed (Munk, 2011). Researchers have resorted to creative and non-conventional measurement systems (aircraft, radar, autosubs, Weddell seals and tethered conductivity–temperature–depth (CTD) profilers) to retrieve observations of the hydrography beneath and adjacent to ice shelves (Corr and others, 2002; Nicholls and others, 2006; Jacobs and others, 2011; Hattermann and others, 2012). Despite the critical role of ice-shelf–ocean systems in changing ice sheets on societally relevant time-scales, direct measurements remain challenging, and our ability to monitor ocean temperature profiles for significant durations of time at even a modest number of sites is limited.

Despite their importance, there remain challenges to developing cost-effective systems for comprehensive monitoring of major sub-ice-shelf cavities. In the mid-1970s, measurements collected beneath the Ross Ice Shelf, Antarctica, at borehole J9 (Jacobs and others, 1979; Foster, 1983) led to fundamental advancements in understanding the hydrographic structure deep within an ice-shelf cavity. Measurements made from moorings in the late 1990s and 2000s (e.g. Nicholls and Makinson, 1998; Nicholls and others, 2001, 2004; Craven and others, 2004; Nicholls and Østerhus, 2004) provided the first year-round observations of temperature, salinity and current conditions beneath major ice shelves. Measurements continue today, including recent data from beneath the Fimbul Ice Shelf (Hattermann and others, 2012), providing even more long-term records of temperature, salinity and currents. In all cases, however, long-term measurements of ocean properties have been limited to discrete points in the vertical and lacked the capability to define the vertical distribution of ocean temperatures in a near-continuous manner.

Generally speaking, environmental and ocean temperature sensing can be broadly divided into two conceptual categories: point-in-space measurements and point-in-time measurements (Tyler and others, 2009). Fixed arrays of temperature sensors (e.g. from moorings) provide point-in-space measurements of water column temperatures at specific depths, predetermined by sensor spacing. Such installations provide excellent temporal resolution of ocean temperature changes at specified depths, but cannot provide a full profile of the temperature distribution. For example, the migration of a thermocline can only be detected when it passes over one of the sensor depths. As multiple sensors are
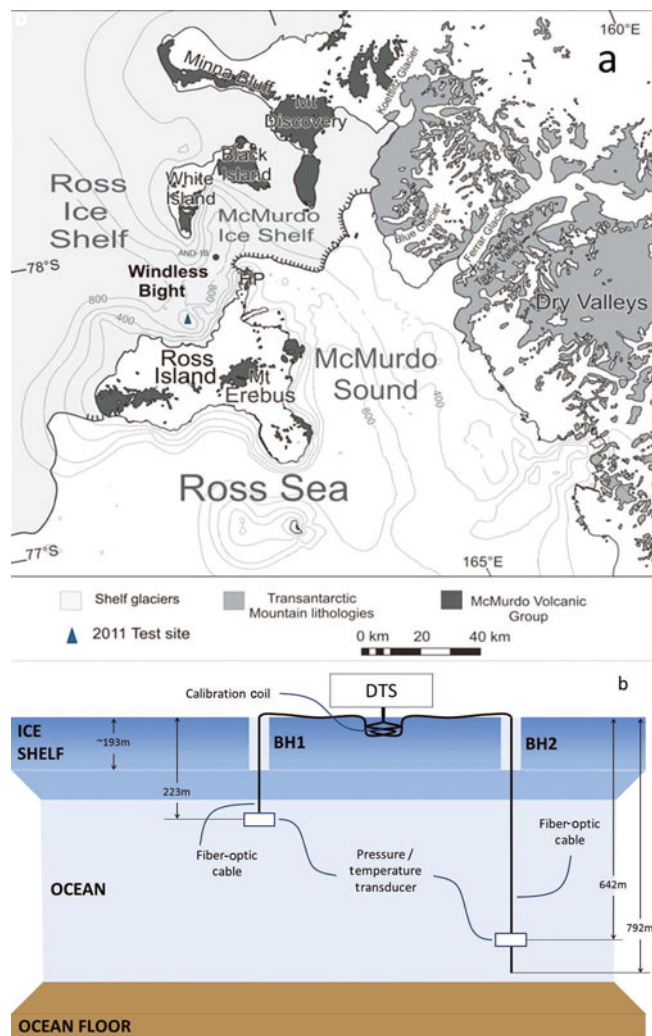
Fig. 1. (a) Location of Windless Bight study site in relation to Ross Island and (b) schematic of moorings BH1 and BH2 through the McMurdo Ice Shelf at Windless Bight.

utilized, care must also be taken to eliminate bias between sensors if temperature gradient information is to be retrieved.

Point-in-time measurements, such as CTD casts, provide a complete vertical profile of the ocean's thermal state and other properties but are limited to the time of measurement. Profilers, either tethered or free-floating such as the Argo floats, can provide a much higher temporal scale of measurement; however, their frequency of profiling may be constrained by onboard power in a sub-ice-shelf environment and by frazil-ice formation (Toole and others, 2011; personal communication from T. Stanton, 2011). Acoustic tomography and inverted echo sounders (IESs) (Rossby, 1969; Meinen and Watts, 2000) perhaps come closest to measuring continuously in both space and time, and have been used to measure ocean thermal and circulation state (Donohue and others, 2010). IES use beneath ice shelves may be a plausible monitoring strategy; however, it will be challenging as these instruments must be placed on the sea floor, powered and monitored.

In all of the systems described above, there are significant challenges to deployment and continuous temperature profiling beneath an ice shelf. In all cases, the system reliability is constrained by instruments that cannot be retrieved or recalibrated once they are placed below the ice shelf. An optimal thermal sensing system will utilize passive sensing (e.g. acoustic tomography) combined with a calibration algorithm that can be located on the accessible ice shelf.

Recent advances in fiber-optic temperature measurement or distributed temperature sensing (DTS) represent a promising new tool for continuous ice-shelf and sub-ice-shelf monitoring. DTS relies on the relation between Raman backscatter intensities in optical fibers and the thermal energy state of the scattering site. Following the 'launch' of a pulse of coherent light down an optical fiber, interactions between the light and the solid are characterized by a variety of elastic and inelastic scattering. The Raman anti-Stokes backscatter intensity, an inelastic interaction, is strongly dependent upon the temperature of the scattering site, while the Raman Stokes backscatter intensity is far less affected by thermal conditions. The scattering site temperatures are calculated from the ratio of the number of backscattered Stokes to anti-Stokes photons rather than the absolute magnitude of either backscatter intensity. As the ratio of backscatter is used, changes in laser intensity, photon density or sensor electronics can be tolerated during deployment. When combined with time-of-flight measurements, DTS provides nearly continuous measurement of fiber temperature over ranges of up to 30 km (Selker and others, 2006). Unlike traditional thermal sensors, DTS provides a continuous (in distance) measurement of fiber temperature over a fixed integration time. As fiber-optic cables can be designed to have small thermal mass, the fibers quickly (<1 min) equilibrate to the temperature of their surroundings and provide a robust measure of most environmental temperatures.

DTS systems have been widely used for industrial applications and have recently been applied to environmental monitoring (Selker and others, 2006; Tyler and others, 2009). Typical DTS systems report temperatures integrated along each 1–2 m of optical fiber using temporal scanning rates of 1–60 s. The potential for DTS in ice-shelf settings has also been demonstrated recently on the Amery Ice Shelf (Warner and others, 2012), demonstrating the feasibility of fiber installation through hot-water-drilled holes and the ability to retrieve ice-shelf and ocean temperatures during instrument deployment over several weeks. DTS temperature resolution can approach 0.03°C over integration times of 60–300 s, providing near-continuous (in depth and time) measurement of ice and ocean temperatures. As the backscatter intensity is transmitted back to the sensing platform optically, all electronics and data processing/storage can be located on the ice-shelf surface and easily serviced. Furthermore, DTS can use commercial small-diameter fiber-optic communication cables, which can be installed easily in relatively small-diameter boreholes through the ice shelf. Such cables are routinely used in harsh and corrosive environments and are therefore well suited to use in both ice shelves and deep ocean settings.

In November 2011, a series of borings through the McMurdo Ice Shelf were completed in order to install two DTS moorings (1) to test their feasibility in a realistic ice-shelf/cavity environment and (2) to develop a long-term remote ice-shelf/cavity temperature monitoring system. In this work, we present data demonstrating the application of DTS measurements of ice-shelf/cavity temperatures collected continuously in both time and depth and discuss the lessons learned from the first season of operation.

STUDY SITE DESCRIPTION

The McMurdo Ice Shelf is located 25 km east of McMurdo station and is contiguous with the much larger Ross Ice Shelf (Robinson and others, 2010). Our study site was located at Windless Bight (Fig. 1a; 77°46.550′ S, 167°32.400′ E) close to several previous oceanographic profiling investigations (Robinson and others, 2010; personal communication from T. Stanton, 2011) and ~20 km from the ice-shelf front. The site provided conditions of ice-shelf thickness, ocean depth, operating temperatures and currents that are common to many shelf glaciers and also allowed straightforward logistical access from McMurdo station.

Two shelf boreholes, BH1 and BH2 (Fig. 1b), were drilled vertically through ~193 m of ice shelf to the ocean using a two-person drilling team. The boreholes were separated horizontally on the surface by 40 m. Through the upper portion of the ice shelf, an electromechanical core drill was used to provide a 135 mm diameter open hole that remained dry through the drilling period. The electromechanical drill was only designed to operate under dry conditions; for final penetration through the last few meters of ice a 40 mm diameter hot-point drill was used. The hot-point drill typically consumed ~3 kW. The total weight of the entire drilling system, including power generation and fuel, was ~400 kg, and each penetration of the ice shelf required ~3 days.

The combination electromechanical plus hot-point drilling system required relatively precise (±2 m) knowledge of the shelf thickness as the electromechanical core drill would be seriously damaged or destroyed by contact with sea water. The hot-point drill was also only designed to penetrate the final 10 m of ice due to the potential for refreezing within the borehole. While ice thickness estimates from radar and drilling data were available from previous fieldwork (personal communication from S. Anandakrishnan and T. Stanton, 2011), these estimates were subject to uncertainty (±10% in the case of radar-derived thickness) and the possibility of changes in shelf thickness since the previous measurements.

To accurately estimate the ice-shelf thickness, periodic measurements of the temperature distribution within the borehole were made by lowering the fiber-optic DTS cable into the dry hole and measuring the temperature profile. A full log of the temperatures in the borehole could be made within several minutes. By extrapolating the observed nonlinear temperature profile in the ice shelf to the freezing temperature of sea water, an estimate of the remaining depth to the ice–ocean interface could be made. In the case of BH1, hot-point drilling was used for the final 7 m, whereas at BH2 the hot-point drill was used for the last 2.5 m of ice.

Upon penetration into the ice-shelf cavity, the hot-point drill was removed from the hole, and sea water rapidly filled to a depth of ~37 m below the ice-shelf surface. BH1 penetrated 192.7 m of ice and BH2 192.9 m; both thicknesses are consistent with observations made from hot-water drilling near the site in 2009 (personal communication from T. Stanton, 2011).

MOORING INSTRUMENT AND INSTALLATION

The boreholes were subsequently instrumented with DTS fiber-optic cables, traditional resistance temperature devices (RTDs) and pressure transducers, all attached to the armored DTS cable. These cables and sensors were lowered through each open hole and allowed to freeze in place. They are subsequently described as 'moorings'. The installation technique was designed to be completed in less than 20 min, the minimum time calculated for refreezing. Analysis of the data showed that the presence of sea water significantly increased the freezing time, allowing access to the ocean for at least 45 min. The maximum sensor diameter was limited to 20 mm to ensure safe passage through the 40 mm diameter hot-point hole.

BH1 was used as a test bed for the installation. The sensing cable was deployed through the open borehole to a depth of 30 m below the ice–ocean interface. The fiber-sensing cable (BruSense, Brugg Kable, Brugg, Switzerland) contained four multimode 50/125 µm optical fibers in a stainless-steel capillary tube to eliminate sea-water pressure stress on the fibers. The capillary tube was further strengthened by stainless wire wrap and a jacket of polyamide to make a final diameter of 3.8 mm and a total weight of 28 kg km^{-1}. At depth, the fibers are joined in a 'turnaround' with bend-optimized fiber in a duplex mode and can be analyzed in either single- or double-ended mode (Tyler and others, 2009).

The mooring package additionally contained an independent recording pressure transducer/thermistor (LevelT-ROLL 700, In-Situ, Inc., Fort Collins, CO, USA; stated accuracy at full scale 0.055°C; resolution 0.003°C) tied to the fiber-optic cable at a depth of 222.7 m below the ice-shelf surface (30 m below the ice–ocean interface at a water depth of ~186 m). This provided both an independent temperature measurement for DTS calibration and an indication of mooring swing. The transducer was connected to the surface with seven-conductor waterproof cable with a diameter of 6.7 mm and a weight of 46 kg km^{-1}.

The bottom end of the fiber-optic cable assembly, including the turnaround, was sealed in a small-diameter waterproof housing, which was also used as the attachment point for the weight system. The mooring weight consisted of three 1 m sections of 20 mm diameter lead-filled steel pipe. Each weight section was 3 kg for a total combined weight of the mooring of ~25 kg.

Additional independent 100 Ω platinum resistance temperature detectors (PT100s), logged by the DTS system, were installed with ~50 m of fiber-optic cable at the surface, horizontally buried in ice at 1.5 m depth to form a long section of fiber at a known and uniform temperature and commonly referred to as a 'calibration coil'. These PT100s were calibrated against a Fluke 1524 (Fluke Corp., Everett, WA, USA) prior to deployment, yielding an accuracy of 0.05°C over the range –10 to +10°C.

Mooring BH2, located 40 m north of BH1, was instrumented with two fiber-sensing cables, the first passing through the ice shelf and extending only 10 m below the ice–ocean interface (BruSense, Brugg Kable, Brugg, Switzerland). Robinson and others (2010) observed maximum tidal currents of ~0.2 m s^{-1} beneath the ice shelf near Windless Bight. This first sensing cable was installed to be subjected to limited tidal stresses and primarily to provide ice-shelf temperatures in the event that the longer cables failed due to repeated flexing by tides and currents.

Mooring BH2 also utilized a second, longer cable extending 792 m below the ice-shelf surface. This cable (DNS-3753, AFL Telecommunications, Duncan, SC, USA) consisted of two 50/125 µm multimode temperature-sensing fibers as well as two 9 µm single-mode fibers encapsulated in a single stainless-steel capillary (2.4 mm outside diameter). The cable was further strengthened by braided stainless wire and finished with a jacket of polyethylene to

give a finished diameter of 6.0 mm and a weight of 65 kg km^{-1}. This mooring was additionally outfitted with 9 kg of weight at the bottom of the cable for a total combined weight of the mooring of ∼70 kg.

The mooring was suspended ∼600 m into the ice-shelf cavity and extended to within an estimated 300 m of the ocean floor (Robinson and others, 2010). Similar to mooring BH1, a recording pressure transducer/thermistor with a maximum pressure rating of 6800 KPa (1000 psi) was tied to the mooring, but at 150 m above the end of the mooring (∼605 m below sea level), and four additional PT100s logged by the data logger were installed in the upper 40 m of the ice shelf at depths of 2.5, 22.5, 32.5 and 37.5 m below the ice surface. These PT100s were not calibrated prior to deployment but were cross-checked in the field against the calibrated PT100s on the DTS. Figure 1b shows a schematic of the completed instrumentation at Windless Bight.

All sensors were connected to a central data collection/ storage/transmission system on the ice surface. In addition to the four-channel DTS laser and Raman detection system (Sensornet Oryx, Sensornet, SA, Elstree, UK), a hardened low-power PC (Eurotech Isis, Eurotec, Inc., Columbia, MD, USA) stored DTS data (on SD cards) and subsequently transmitted compressed data to a data logger (CR3000, Campbell Scientific, Logan, UT, USA). The data logger also monitored the transducers and PT100s, along with power management data. All independent sensors were recorded at 10 min intervals through the deployment, with DTS measurements made eight times per day from November through March and four times per day after mid-March to conserve power. Power is supplied to the system via a combination of batteries, photovoltaic panels and a wind turbine. The total power consumption for the system when operating in winter-sampling mode was <8 W.

The system further included a series of current-measuring Hall effect devices to monitor current draws of each of the major instruments, as well as solar power and wind generator amperage. The power monitoring system was also designed with a series of relays to allow remote switching and reboot capability via the data logger. The datasets are transmitted eight times a day via an Iridium modem and stored on a dedicated server in North America.

DTS DATA PROCESSING

Raman scattering returns were integrated over 5 min intervals from one or more fibers in each cable. The DTS interrogator integrates Raman photons over ∼1 m increments along the cable and has been shown to have a spatial resolution of 2.06 ± 0.05 m (Suárez and others, 2011). This spatial resolution represents the length required to record 80% of a step change in fiber temperature (Tyler and others, 2009). Field-derived Raman backscatter intensity was combined with independent temperature measurements from the PT100s in the calibration coil and from thermistors within the water column to calculate the independent parameters relating Raman return intensity to fiber temperature via

$$T(z) = \frac{\gamma}{\ln \frac{P_s}{P_{aS}} + C - \Delta\alpha z} \tag{1}$$

where γ represents the energy shift in photons between incident and scattered Raman photons, P_s and P_{aS} represent the intensity of the Stokes and anti-Stokes backscatter, respectively, C is a dimensionless parameter including proper-

ties of both the source laser and the DTS instrument, $\Delta\alpha$ represents the differential attenuation coefficient between anti-Stokes and Stokes photons within the fiber, and z represents the position along the cable at which scattering occurs (Hausner and others, 2011). Assuming each of the coefficients is unknown (and independent of space in the case of $\Delta\alpha$), Eqn (1) requires three independent temperatures to be known in order to calculate temperatures along the fiber-optic cable.

Ocean and ice-shelf temperatures were calibrated separately, as ocean temperatures varied by <0.8°C over the course of the season, while ice-shelf temperatures varied as much as 20°C in the vertical. Ocean temperature calibration utilized both transducers within the water column, along with one section of calibration coil buried at the surface close to the laser source. Ice-shelf calibration utilized an additional PT100 near the firn–ice transition to better span the wider range of temperatures found in the ice shelf. Interpolation was used to fill data gaps in the records, primarily from the transducer records.

Calibration parameters (Eqn (1)) varied only slightly from one time trace to the next. For calibration of the ocean profile, both differential attenuation, $\Delta\alpha$, and γ varied by <2% over the entire data collection period ($8.5 \times 10^{-5} \pm 0.2$ m^{-1} and 480 ± 8 K, respectively) while C, representing both laser and electronic variation, showed the widest range of variation at ∼5%. This was also recorded in the variation in laser source power, which varied by as much as 10% over the course of the experiment. However, laser power has little impact on temperature resolution, as it is the ratio of Raman Stokes to anti-Stokes scattering that determines the calculated temperature, not the absolute magnitude of either return signal.

All ocean temperatures reported in this work have been subsequently corrected for adiabatic expansion (conservative temperature, TEOS-10; www.teos-10.org) referenced to sea level. Since direct measurements of salinity during the deployment are absent, a uniform absolute salinity of 35 g kg^{-1} was assumed. Salinity variations with depth of ∼0.3 psu have been reported previously in the region (Robinson and others, 2010; Mahoney and others, 2011), but these variations equate to conservative temperature differences at least one order of magnitude smaller than the resolution of the DTS temperature measurements. The depth used to convert each measurement to conservative temperature was estimated by linearly extrapolating pressures reported from the two sub-ice-shelf transducers to account for mooring swing. During gaps in the transducer record, the moorings were assumed to be vertical.

While the observed pressure was used to convert to conservative temperatures, we choose to report the depth of the DTS measurement as the measured distance along the mooring, without correction for mooring deviation in time. Only one deep measurement of the mooring depth was available to make a deviation correction and, as discussed below, the moorings showed most vertical deviation early in the deployment.

RESULTS
Ice-shelf thermal profiles

As described above, ice-shelf temperatures were measured using a temporary DTS fiber prior to penetration into the ocean to precisely estimate ice-shelf thickness. Immediately after penetration of the ice–ocean interface, logging of

mooring BH1 was initiated for ~42 hours to monitor the freezing process and to investigate the time needed for re-equilibration of the ice-shelf temperatures to their original profiles.

Figure 2 shows the time evolution of temperatures prior to, during and well after freeze-in of this first mooring. After several months (Fig. 2; solid blue trace) the ice-shelf temperature profile is nonlinear and consistent with previous observations of Antarctic ice shelves (e.g. Budd and others, 1982). The DTS provides a nearly continuous profile in space, in which the dominant heat transfer mechanisms (melting from below, accumulation rate above, etc.) can be investigated more precisely than with only a few measurement points available to constrain the functional form of the solution.

To the right of the equilibrated profile in Figure 2 are four traces of ice-shelf temperature taken immediately after installation of the fiber-optic cable into the ice shelf ($t = 0$) and at 5, 8 and 18 hours after insertion. Immediately after penetration of the ocean, the shelf temperatures represent that of the underlying ocean (at a depth of 193 m below the ice surface) and the sea-water–air interface is represented by the large change in temperature at ~37 m below the ice surface. Over time, the borehole freezes and temperatures revert to the pre-penetration temperature profile. However, this relaxation to equilibrium is far from uniform in time or depth, as is shown in Figure 2. Near the bottom of the shelf, a step change to lower temperatures is evident and reflects the difference in borehole diameter in this lower region. As the deepest portion of the borehole was only 40 mm in diameter, its freezing and subsequent re-equilibration with the surrounding ice shelf is faster than the larger-diameter region above it.

Also clearly visible is the development of temperature reversals which form, grow and eventually diffuse over the 2 day intense monitoring period. These are possibly formed by local convective zones, driven by brine rejection during freezing and heat loss to the walls. While there was sufficient 'freeze' to anchor the moorings into the ice after only 5 hours, it is clear that complete freezing took much longer and that return to equilibrium conditions in the ice shelf requires timescales of weeks to months. The observation that such small-scale features can be resolved indicates that the potential for monitoring long-term ice-shelf temperature perturbations using DTS may be quite significant.

Sub-ice-shelf thermal profiles

Sub-ice ocean monitoring began in late November 2011 and continued through late June 2012. The system operated nearly continuously from late November 2011 through the end of June 2012, when an unanticipated drop in available electrical power caused the system to shut down. Here we present data only from the deepest DTS mooring to illustrate water column responses. From November 2011 through mid-March 2012, eight ocean profiles were recovered daily from BH2; each profile was collected over a 5 min averaging window. After March 2012, the sampling frequency was reduced to four times per day to conserve electrical power. Twelve periods of DTS data gaps occurred over this period, ranging from 1 to 14 days. Most gaps were short (1–4 days) and were resolved by automatic rebooting of the system. The longest data gaps (December and March, 9 and 14 days, respectively) were associated with programming errors on the DTS and the data logger. Since November 2011,
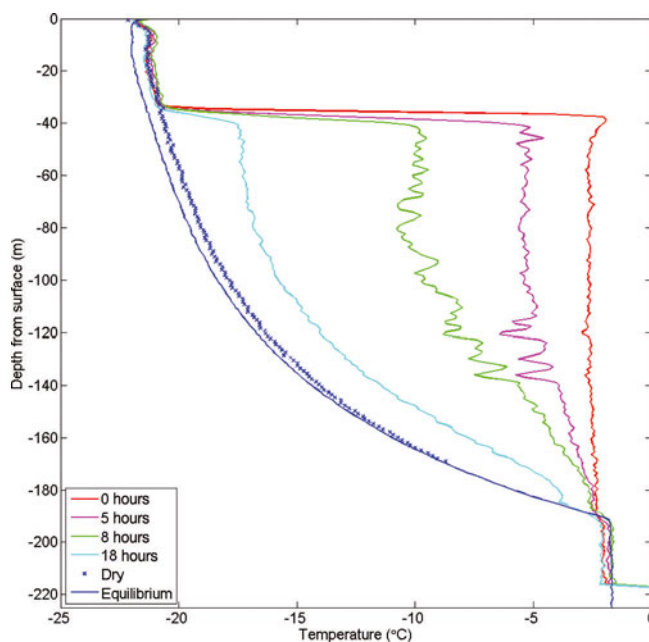

Fig. 2. Selected ice-shelf temperatures during the austral summer of 2011/12. The trace denoted by blue crosses was measured in BH1 prior to the borehole penetrating the ice–ocean interface, while the solid blue trace is representative of ice-shelf temperatures several months after refreezing and equilibration. The slight differences between the pre-penetration temperature and the assumed equilibrium profile are due to drilling perturbations and a limited availability of independent calibration temperatures during the first days of installation. The trend of the traces to lower values with time represents temperatures measured immediately after fiber installation (red) and 5, 8 and 18 hours after lowering of the mooring through the ice shelf when liquid water was still present in the borehole.

~3×10^6 temperature measurements to a depth of ~743 m below the ice surface have been collected. Figure 3 shows only the ocean temperature profiles from BH2 for clarity, with assumed vertical depth below sea level as the vertical axis.

As anticipated, the ocean temperatures beneath the ice shelf in November and December are nearly uniform with depth (Robinson and others, 2010; Mahoney and others, 2011). Warm water incursion began in mid-January, forming a thickening and warming layer at the ice–ocean interface. This is ~3 weeks after the onset of warming near the edge of the McMurdo Ice Shelf at Cape Armitage reported in the 2008/09 season (Mahoney and others, 2011). This wedge of warm water reaches its maximum depth of ~150 m beneath the ice–ocean interface by mid-March and then begins to retreat. The maximum temperature reached at the ice–ocean interface is –1.15°C. The entrance and departure of warm water from McMurdo Sound is not uniform in time, particularly at the onset of warming in January. The maximum warming beneath the ice shelf occurs in early March, with retreat of the bulk of warm water by mid-April. These profiles and the associated oceanographic interpretation will be discussed in detail in a later paper (A.A. Stern, S.W. Tyler, V. Zagorodnov, M.S. Dinnimin and D.M. Holland, unpublished data).

Mooring deviations

To record possible mooring swings due to currents or formation of frazil ice, the depths of the moorings were monitored at 186 m below mean sea level on mooring BH1 and 605 m below mean sea level at mooring BH2. Figure 4a
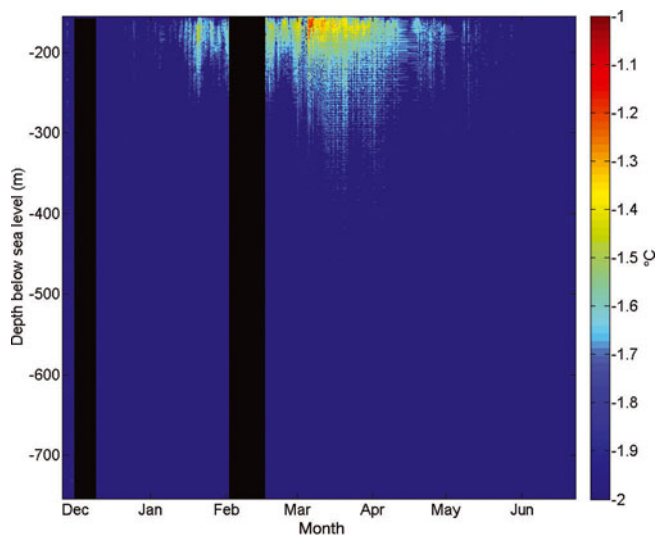
Fig. 3. Compilation of sub-ice-shelf ocean temperatures from late November 2011 through June 2012 as recorded via DTS. Temperatures are reported as conservative temperature, and depths are reported as distance below sea level along the mooring. The longest data gaps are shown in black, while several shorter data gaps in April and May appear as periods of constant temperature.

shows the observed depth of the BH2 mooring transducer. Almost immediately after deployment the deepest portion of mooring BH2 was observed to rise almost 150 m, with continued rises through December. Figure 4b expands the early-season mooring depth excursions, with each mooring swing occurring over a period of 12–48 hours. In contrast, mooring BH1, penetrating only 30 m into the ocean, varied in depth by <1 m over this same period (data not shown). Measured tidal currents nearby were as high as 0.2 m s^{-1} in previous seasons (Robinson and others, 2010) and are sufficient to induce drag on both moorings to cause the observed swings. However, the longer-period swings and decrease in amplitude as warm water intruded into the cavity suggest that formation of frazil ice on the moorings may have further contributed to the swings, particularly in mooring BH2. Frazil ice on rope moorings was observed by Mahoney and others (2011) adjacent to the edge of the McMurdo Ice Shelf in late winter. The total weight (in air) of mooring BH2 was only ~70 kg ($\rho \sim 2000$ kg m^{-3}), and formation of a 50% porosity frazil-ice 'rind' of ~6 cm diameter was sufficient to neutralize the mooring buoyancy. This rind would also significantly increase current drag on the mooring. Although the transducer record is not complete after March, Figure 4a suggests mooring swings greatly decreased after February, coincident with the arrival of warmer water beneath the shelf and potential elimination of frazil-ice conditions. Both moorings were still subjected to tidal currents after February; however, it appears that without frazil ice on the mooring, the small cross-sectional area of the mooring and negative buoyancy reduced the impact of currents on the moorings.

Performance of the remote system

The monitoring system consisted of five primary components: DTS interrogator, sensing fiber-optic cable, data acquisition/storage and communications, supplementary sensors and power supply (battery bank) and generation (solar and wind). We now provide a brief summary of the performance of each of the major components to aid the design of future long-term deployments.
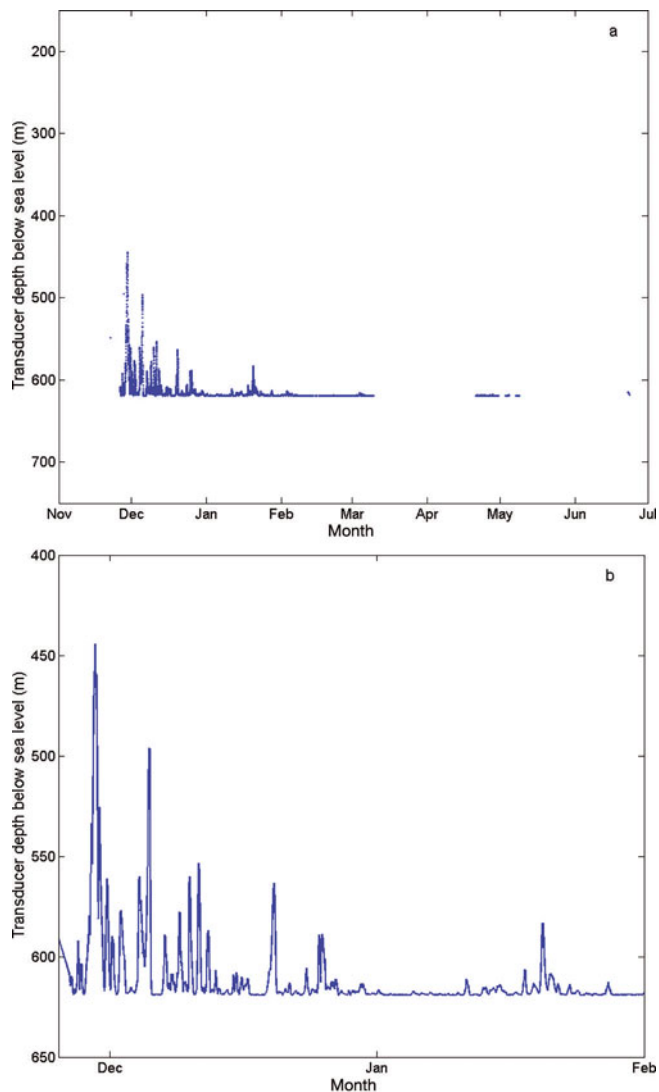

Fig. 4. (a) Depths recorded from mooring BH2. The large changes in depth are likely the result of current drag on the moorings, potentially enhanced by the formation of frazil ice on the mooring. (b) An expanded view of the period of largest swings early in the deployment. These swings are not at tidal periods but typically last 12–48 hours. The reported submergence depth of the transducer is based on an ocean column of uniform density.

The DTS, along with most of the system hardware, was automatically rebooted once a day as this is known to be useful in cold-region applications. With the exception of short data gaps, the DTS data provided high temporal resolution. Power use by the DTS was optimized by only powering for measurement cycles four times per day (20 min cycle^{-1}) during winter. During idle times, the DTS consumed <0.5 W.

Although DTS can provide high spatial resolution of ocean and ice temperatures, estimation of its temperature accuracy and resolution must be assessed. DTS infers temperature from photon-scattering events, and absolute accuracy is therefore ultimately controlled by the absolute accuracy of the independent temperature sensors used in calibration. The two independent PT100 temperature sensors on the DTS were calibrated prior to deployment over a laboratory range of –10 to +10°C and had accuracies of 0.05°C and 0.055°C. The three-point calibration of Hausner and others (2011) forces the DTS temperatures in the

calibration sections to match exactly the independently measured temperatures, so the calibrated DTS temperatures have no bias within the three calibration sections. Since the three calibration sections were located at the beginning, approximate middle and near the end of the mooring, bias outside these sections is unlikely to occur unless the sensing cable is damaged. The absolute accuracy of the calibrated DTS temperatures in the ocean profile can therefore be considered to be ±0.055°C, the least accurate of the independent temperature sensors used for the ocean calibration. The ice-shelf profile is less accurate than that of the ocean profile as the PT100 at the firn–ice transition was not calibrated to the same level of accuracy prior to deployment.

Equally important for ice-shelf and ocean dynamics is the ability to resolve differences in temperature. DTS temperature resolution is typically calculated from the root-mean-square error (RMSE) of ≥20 temperature measurements made over a section of fiber at uniform temperature (Hausner and others, 2011). The resolution degrades with distance down the fiber as fewer photons are available for scattering. In this deployment, there was only one section of fiber at the surface that could be assumed to be at uniform (in space) temperature and this was relatively close to the sensing system. To estimate resolution at both the start and end of the mooring, we assumed that a 20 m interval across the deepest pressure transducer could be considered to be at uniform temperature during each DTS trace. While an assumption, the calculated standard deviation over the deployment of this deepest independent temperature measurement was ~0.002°C, implying that temperature at this depth was essentially constant. This lack of temperature variation at depth was also supported by the previous season's data from adjacent to the McMurdo Ice Shelf (Mahoney and others, 2011).

Using this model of resolution, the DTS temperature resolution ranged from 0.024°C in the calibration coil near the sensor to 0.030°C at a distance of 742 m down the fiber. These calculated resolutions are consistent with the instrument manufacturer's stated resolutions for 5 min integration times at distances of 100 and 1000 m. Absolute accuracy in future deployments can be improved by using more sophisticated temperature sensors located on the surface where they can be recalibrated, and additional temperature sensors along the mooring. Improvements in resolution are now available commercially, but can also be made with longer integration times.

A major concern for long-term monitoring is the ability of the fiber-optic cables to withstand strain and repeated bending due to current swings or freezing. Strain on fibers increases their light attenuation and can also induce differential attenuation in the Stokes and anti-Stokes return signals, reducing the ability of the DTS system to resolve temperatures accurately. While these fibers were designed to be isolated from radial strain due to ocean pressure, flexing or twisting of the cable can induce bending strains on the fibers. Attenuation typically follows Beer's law and is calculated as the ratio of backscatter from two regions of the fiber separated by a known distance, typically calculated as $-10 \log_{10}(P1/P2)$ where $P1$ and $P2$ represent the backscatter intensity at the upstream and downstream positions, respectively. Figure 5 shows the attenuation (dB km^{-1}) for three uniform temperature sections of mooring BH2 that were subjected to differing strains: freezing of the calibration coil at the surface (blue), at the bottom of the mooring (red)
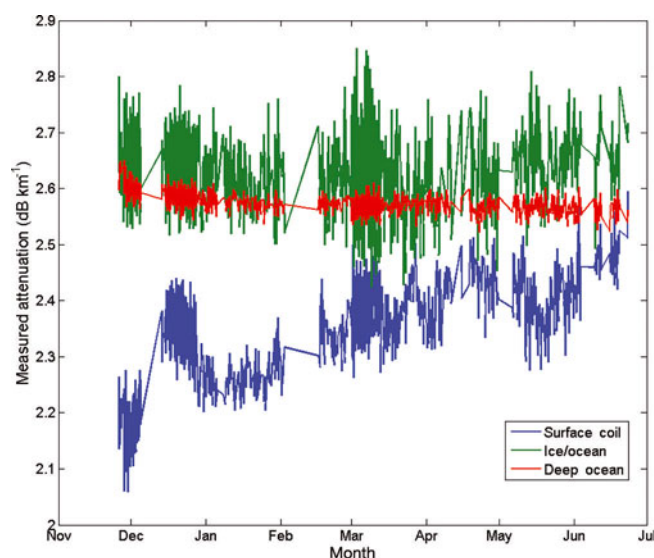

Fig. 5. Measured attenuation (dB km^{-1}) for three representative sections of the cable in mooring BH2. While the ice–ocean (green) and deep ocean (red) portions of the fiber do not show significant time-varying strain, the portion of the cable at the surface (blue) increases in attenuation early in the deployment, suggesting that freezing of the calibration coil may have caused some fiber strain.

and directly below the ice–water interface (green). The calibration coil was exposed to the greatest potential for radial strain during freezing as well as some bending strain as the ice block in which it was installed slowly froze and cooled, while the fiber at the ice–ocean interface was likely to be subjected to the greatest bending and flexing strain during tides or current swings. The fiber at depth would be affected by radial strain due to sea-water pressure only if the watertight seal became compromised or if the capillary tube containing the fibers was crushed or damaged.

Several observations can be made from Figure 5. First, the overall magnitude of attenuation (2.0–2.5 dB km^{-1}) is consistent with unstrained multimode fiber for wavelengths used in the DTS (~1000 nm); therefore, no major strain appears to have been put on any of these fibers over the course of the deployment. Furthermore, temporal change in attenuation was not observed in the fibers in the ocean column, indicating flexing and bending did not cause any failure or breaks in the integrity of the capillary tube containing the fibers or at the turnaround junction. There is much greater variability in the calculated attenuation for the portion of the cable near the ice–ocean interface, but this is caused primarily by the fact that the temperature of the two sections of fiber used to calculate the attenuation were not the same over time, particularly after mid-January, and will result in errors in attenuation calculation.

Most interesting is the attenuation behavior of the cable at the surface, where a series of cable loops is placed into an initially water-filled container to serve as a calibration section of fiber. This section appears to have undergone some time-dependent strain over the course of the monitoring, as the attenuation increases from ~2.0 to ~2.6 dB km^{-1}. In this case, the strain may be the result of slow contraction of the ice in the container as it cooled into the winter, localized strain from an initial bend in the cable that was accentuated by freezing or other causes. This observation suggests that future installations will benefit from greater isolation of the fibers from freezing strain and greater care when coiling a

cable that may freeze, which could be accomplished with strain-absorbing materials within the cable itself or through the use of non-freezing solutions.

The data acquisition/storage and communications systems performed adequately throughout the deployment. Communication via Iridium connection had sufficient bandwidth to transmit up to 10 MB data daily through much of the experiment period. Typical data transmission was designed to require 1–2 MB d^{-1}, including redundant data and system performance data transmission for this first test of the system. This would not be necessary in future deployments. Future deployment bandwidth needs are anticipated to be 10–100 KB d^{-1}, which can be accomplished with onboard data processing and further data compression. For example, much of the ice-shelf profile is unchanging in time and could be transmitted weekly without loss of information.

The power supply and power generation system performed as designed through June 2012. The battery supply voltage dropped below minimum levels in late June 2012 and the system shut down. However, by mid-September 2012 the photovoltaic panels had recharged the battery system sufficiently and the system is operational at the time of writing. The reason for the drop in battery voltage does not appear to have been related to the DTS. The entire system is to be returned to our laboratory in January 2013 for post-deployment diagnostics.

CONCLUSIONS

Nearly continuous (in time and depth) profiles of temperature have been made through and beneath an ice shelf. The measurement system, DTS, is capable of operating in the harsh environments of ice shelves, and resolving temperature through the ice shelf and cavity. Unlike traditional CTD sensors, measurements are made continuously along the fiber-optic cable and depend only on the light-scattering properties of the fiber. Instrumentation can be housed on the surface, with limited power demands, and can be recalibrated or serviced. In addition, the instrumentation can be installed via very small (<40 mm) diameter boreholes through the ice shelf, reducing the logistical support and time needed to install the systems in remote locations.

The DTS temperature resolution (20–30 mK) currently is not fully comparable with modern oceanographic instruments, which can resolve to 1 mK, but can be improved with longer sampling times and recent advances in instrument design. Spatial resolution can also be increased either by changing the geometry of the mooring (Selker and others, 2006; Suarez and others, 2011) or by improvements in the DTS data acquisition systems. When used in conjunction with other sensing platforms, including higher-resolution thermal probes, salinity and current sensors, DTS can provide much higher spatial resolution of thermal processes than has been previously available for oceanographic and ice-shelf monitoring.

REFERENCES

Budd WF, Corry MJ and Jacka TH (1982) Results from the Amery Ice Shelf Project. *Ann. Glaciol.,* **3**, 36–41

Corr HFJ, Jenkins A, Nicholls KW and Doake CSM (2002) Precise measurement of changes in ice-shelf thickness by phase-sensitive radar to determine basal melt rates. *Geophys. Res. Lett.,* **29**(8), 1232 (doi: 10.1029/2001GL014618)

Craven M and 6 others (2004) Initial borehole results from the Amery Ice Shelf hot-water drilling project. *Ann. Glaciol.,* **39**, 531–539 (doi: 10.3189/172756404781814311)

Donohue KA, Watts DR, Tracey KL, Greene AD and Kennelly M (2010) Mapping circulation in the Kuroshio extension with an array of current and pressure recording inverted echo sounders. *J. Atmos. Ocean. Technol.,* **27**(3), 507–527 (doi: 10.1175/2009JTECHO686.1)

Foster TD (1983) The temperature and salinity fine structure of the ocean under the Ross Ice Shelf. *J. Geophys. Res.,* **88**(C4), 2556–2564 (doi: 10.1029/JC088iC04p02556)

Hattermann T, Nøst OA, Lilly JM and Smedsrud LH (2012) Two years of oceanic observations below the Fimbul Ice Shelf, Antarctica. *Geophys. Res. Lett.,* **39**(12), L12605 (doi: 10.1029/2012GL051012)

Hausner MB, Suárez F, Glander KE, Van de Giesen N, Selker JS and Tyler SW (2011) Calibrating single-ended fiber-optic Raman spectra distributed temperature sensing data. *Sensors,* **11**(11), 10 859–10 879 (doi: 10.3390/s111110859)

Hellmer H, Kauker F, Timmermann R, Determann J and Rae J (2012) Twenty-first-century warming of a large Antarctic ice-shelf cavity by a redirected coastal current. *Nature,* **485**(7397), 225–228 (doi: 10.1038/nature11064)

Jacobs SS, Gordon AL and Ardai JLJ (1979) Circulation and melting beneath the Ross Ice Shelf. *Science,* **203**(4379), 439–443 (doi: 10.1126/science.203.4379.439)

Jacobs SS, Jenkins A, Giulivi CF and Dutrieux P (2011) Stronger ocean circulation and increased melting under Pine Island Glacier ice shelf. *Nature Geosci.,* **4**(8), 519–523 (doi: 10.1038/ngeo1188)

Mahoney AR and 6 others (2011) The seasonal appearance of ice shelf water in coastal Antarctica and its effect on sea ice growth. *J. Geophys. Res.,* **116**(C11), C11032 (doi: 10.1029/2011JC007060)

Meinen CS and Watts DR (2000) Vertical structure and transport on a transect across the North Atlantic Current near 42°N: time series and mean. *J. Geophys. Res.,* **105**(C9), 21 869–21 891 (doi: 10.1029/2000JC900097)

Munk W (2011) The sound of climate change. *Tellus,* **63**(2), 190–197 (doi: 10.1111/j.1600-0870.2010.00494.x)

Nicholls KW and Makinson K (1998) Ocean circulation beneath the western Ronne Ice Shelf, as derived from in situ measurements of water currents and properties. In Jacobs SS and Weiss RF eds. *Ocean, ice and atmosphere: interactions at the Antarctic continental margin.* (Antarctic Research Series 75) American Geophysical Union, Washington, DC, 301–318

Nicholls KW and Østerhus S (2004) Interannual variability and ventilation timescales in the ocean cavity beneath Filchner–Ronne Ice Shelf, Antarctica. *J. Geophys. Res.*, **109**(C4), C04014 (doi: 10.1029/2003JC002149)

Nicholls KW, Østerhus S, Makinson K and Johnson MR (2001) Oceanographic conditions south of Berkner Island, beneath Filchner–Ronne Ice Shelf, Antarctica. *J. Geophys. Res.*, **106**(C6), 11 481–11 492 (doi: 10.1029/2000JC000350)

Nicholls KW, Makinson K and Østerhus S (2004) Circulation and water masses beneath the northern Ronne Ice Shelf, Antarctica. *J. Geophys. Res.*, **109**(C12), C12017 (doi: 10.1029/2004JC002302)

Nicholls KW and 21 others (2006) Measurements beneath an Antarctic ice shelf using an autonomous underwater vehicle. *Geophys. Res. Lett.*, **33**(8), L08162 (doi: 10.1029/2006GL025998)

Robinson NJ, Williams MJM, Barrett PJ and Pyne AR (2010) Observations of flow and ice–ocean interaction beneath the McMurdo Ice Shelf, Antarctica. *J. Geophys. Res.*, **115**(C3), C03025 (doi: 10.1029/2008JC005255)

Rossby T (1969) On monitoring depth variations of the main thermocline acoustically. *J. Geophys. Res.*, **74**(23), 5542–5546 (doi: 10.1029/JC074i023p05542)

Selker J, Van de Giesen N, Westhoff M, Luxemburg W and Parlange MB (2006) Fiber optics opens window on stream dynamics. *Geophys. Res. Lett.*, **33**(24), 24401 (doi: 10.1029/2006GL027979)

Suárez F, Aravena JE, Hausner MB, Childress AE and Tyler SW (2011) Assessment of a vertical high-resolution distributed-temperature-sensing system in a shallow thermohaline environment. *Hydrol. Earth Syst. Sci.*, **15**(3), 1081–1093 (doi: 10.5194/hess-15–1081–2011)

Toole JM, Krishfield RA, Timmermans M-L and Proshutinsky A (2011) The ice-tethered profiler: Argo of the Arctic. *Oceanography*, **24**(3), 126–135 (doi: 10.5670/oceanog.2011.64)

Tyler SW and 6 others (2009) Environmental temperature sensing using Raman spectra DTS fiber-optic methods. *Water Resour. Res.*, **45**(4), W00D23 (doi: 10.1029/2008WR007052)

Warner R, Craven M, Galton-Fenzi B, Elcheikh A, Christensen A and Vogel S (2012) Distributed temperature sensing in the Amery Ice Shelf and the sub-ice-shelf ocean. In Hanke M and Kirchner N eds. *Book of Abstracts of 26th International Forum for Research into Ice Shelf Processes (FRISP), 12–14 June 2012, Stockholm Archipelago, Sweden* http://urn.kb.se/resolve?urn=urn:nbn:se:su:diva-88405